

Growth Modelling of *Saccharomyces cerevisiae* and Simulation of Pyrite Ash X-ray Diffraction Patterns

Y. Ermurat

Bolu Abant İzzet Baysal University, Engineering Faculty, Department of Chemical Engineering, Bolu, Turkey

This work is licensed under a
Creative Commons Attribution 4.0
International License



Abstract

Saccharomyces cerevisiae was incubated in media comprising pyrite ash for growth modelling studies, and the samples of pyrite ash were analysed using X-ray diffraction (XRD) to simulate profiles. The sigmoidal modelling curves in 3D growth graphs were presented alongside numerical error computations and graphs. Simulation of XRD spectra of the pyrite ash using diffraction profiling functions were conducted for designing a combined experimental process. The von Bertalanffy growth model function yielded the lowest relative error value of 11.56 %, and the exponential model estimation produced the low numerical error percentages as Euler's error of 4.8 %, and Heun's error of 5.36 %. Gaussian and Lorentzian approximations were applied to shape the data of the XRD profiles of sulphur-containing samples, and well-described graph simulations were obtained using the Gaussian estimation.

Keywords

Saccharomyces cerevisiae, pyrite ash, growth modelling, error analysis, XRD analysis

1 Introduction

Saccharomyces cerevisiae can survive in inorganic mineral sources, such as iron-sulphur mineral pyrite ash medium. Pyrite ash is a discarded material of sulphuric acid manufacturing plants as an iron-sulphur ore by-product. Powdered pyrite ore is calcinated to oxidise its sulphur content into sulphur dioxide gas leaving a mass of depleted mineral ash that contains significant amounts of iron in forms of oxides and trace amounts of sulphides.¹

Chemical and biochemical reactions, as well as the data of biological growth dynamics are usually characterised by sigmoid models, and display sigmoidal curves that exhibit S-shaped graphical lines. Activities of chemical and biochemical catalysts, besides growth of living organisms, present sigmoidal appearances.²

The powder X-ray diffraction (XRD) analysis of pyrite ash indicates that the sulphur residue of pyrite ash is associated with minerals such as FeS, CuS, CuSO₄, PbS, and PbSO₄.^{1,3} The effect of roasted pyrite ash on soil has been evaluated, and the potential risks have been defined.^{4,5}

The nanomineralogical composition of roasted pyrite ash was investigated, and numerous heavy metal elements, such as As, Cr, Cu, Co, La, Mn, Ni, Pb, Sb, Se, Sr, Ti, Zn, and Zr, were determined using XRD, high-resolution transmission electron microscopy, and field emission scanning electron microscopy.³

S. cerevisiae is used for the massive production of single cell protein and ethanol. The growth of *S. cerevisiae* in a pyrite

ash based medium has been examined to analyse the capability of the bacterium to metabolise organic and inorganic sulphur, in addition to its growth progression in mineral media. Inorganic sulphur compounds, as in pyrite ash, can be converted into organic forms through the bioprocess of protein molecules by *S. cerevisiae*. Several studies have revealed that *S. cerevisiae* can assimilate sulphur complexes through specific sulphur pathway systems to produce intracellular sulphur-containing serine, threonine, cysteine, and methionine amino acids, as well as extracellular hydrogen sulphide (H₂S). *S. cerevisiae* possesses special enzymes for use in sulphate-assimilatory metabolism. As *S. cerevisiae* actively produces H₂S during growth, its metabolism and genetics are being extensively studied for investigating the dissimilatory and assimilatory metabolisms of inorganic sulphur compounds. *S. cerevisiae* can use various organic and inorganic nitrogen compounds, thus increasing uptake of the carbon and sulphur substances.^{6–9}

Several studies have been conducted to understand the effect of heavy metals on the survival capability of *S. cerevisiae*. Cadmium toxicity was modelled in the growth process of *S. cerevisiae* from the lag phase to the stationary phase, and the preliminary cell mortality was represented by increasing cadmium levels.¹⁰ In other studies, the biosorption and accumulation of heavy metals by *S. cerevisiae* have been effectively investigated experimentally.^{11–14}

The main objective of this study was to investigate modelling of the growth of *S. cerevisiae* incubated in the media containing pyrite ash by using characteristic growth modelling functions, and to determine the errors between the observed and approximated values. XRD simulation analysis of the structure of pyrite ash samples is planned using diffraction profiling functions.

* Assist. Prof. Dr. Yakup Ermurat
Email: yakupermurat@ibu.edu.tr

2 Materials and methods

S. cerevisiae was isolated from commercial baker’s yeast and incubated starting with an initial count (N_0) of $1 \cdot 10^5$ CFU ml⁻¹ according to selective isolation and incubation methods. The samples of pyrite ash with high iron (61.08 %) and low sulphur (0.59 %) contents were supplied from the calcinated waste ashes of the Eti Mining Bandırma Borax Plant in Turkey. Pyrite ash solutions (3 %) were prepared for incubation trials in 40-litre plastic tank, and incubation media were formulated using non-sulphur containing carbon/nitrogen sources as well as glucose, salts, and vitamins. Incubation was performed at an average growth temperature of 37 °C for five days in batch-type liquid-state bioprocesses. Nitrogen and phosphate extracted from the poultry waste into water by the application of CO₂ from the Bolu region were applied as putative substrates for incubation. Isolation and identification procedures of *S. cerevisiae* strains were conducted at the laboratories of the Scientific Industrial and Technological Applications and Research Centre, and mineralogical studies of the pyrite ash samples during experimental investigations were performed using the Rigaku XRD set up at the laboratory of the Physics Department of the Faculty of Literature and Science, Bolu Abant İzzet Baysal University. The XRD profile analysis of pyrite ash samples was performed with the diffraction peaks between 20° and 90° 2θ angles. Modelling functions were used to estimate the predicted counts of *S. cerevisiae*, and calculations, 3D sigmoidal graphs, and profile simulation graphs were assessed using MATLAB software.¹⁵

2.1 Growth model functions

The sigmoid model appropriately describes the growth of organisms with simple life cycles that starts with a sluggish growth, continues with fast-exponential growth, and concludes with declining growth.^{16,17} Characteristic growth models that consider intrinsic rate constants are recognised as useful tools to fit the calculated data with the real data of the sigmoid curves.¹⁸ Some well-known practiced models and their modified forms are the Malthusian exponential, Verhulst logistic, Richards, Gompertz, and von Bertalanffy functions. The functions are modified to investigate the living aspects and growth dynamics of microorganisms in certain experimental or natural conditions. The models and their modified forms with major restrictions were successfully applied to evaluate growth dynamics by fitting the predicted data with the experimented data.^{19–25} The growth model functions and their analytical solutions, which are used to determine the best fitting models for growth processes are listed in Table 1.

The Malthusian exponential growth model function indicates that the current growth of the microorganisms is strictly proportional to the initial population (N_0), although it cannot sufficiently represent entirely restrictive growth parameters. The Verhulst logistic estimation is adjusted for sufficiently characterising the growth restrictions with maximal viability (N_m), which is described as the carrying capacity as a limiting case. The capacity acknowledged as the main parameter, since it depends on population saturation level characteristics and regulates the growth dynamics of organisms. Except the exponential modelling

Table 1 – Growth model functions and their analytical solutions

Growth models	Functions	Analytical solutions
Malthusian exponential	$\frac{dN}{dt} = rN_0$	$N = N_0e^{rt}$
Verhulst logistic	$\frac{dN}{dt} = rN\left(1 - \frac{N}{K}\right)$	$N = \frac{KN_0}{(K - N_0)e^{-rt} + N_0}$
Gompertz	$\frac{dN}{dt} = rN\left[\ln\left(\frac{N}{K}\right)\right]$	$N = K \exp\left[\ln\left(\frac{N_0}{K}\right)\right] e^{rt}$
Richards	$\frac{dN}{dt} = rN\left(1 - \frac{N}{K}\right)^\beta$	$N = K\left[\left(1 - e^{-\beta rt}\right)\left[1 - \frac{N_0}{K}\right]^{-\beta}\right]^{1/\beta}$
von Bertalanffy	$\frac{dN}{dt} = rN^\alpha\left[1 - \frac{N}{K}\right]^\beta$	$N = K\left[1 + \left[1 - \frac{N_0}{K}\right]^\beta e^{-\beta rt}\right]^{1/\beta}$

equation, all the other modelling functions are described as extended logistic equations. Among them, the Richards and the von Bertalanffy functions are Bernoulli-type differential equations, which are considered as estimating the complete growth parameters through modifications of the exponential power type (β). The von Bertalanffy function is an improved form of the Richards function incorporated with $\beta = 3$ power type evaluation.^{23,24}

2.2 Error equations

The accuracy of the approximated data set generated from the modelling equations can be obtained through an error analysis, representing the deviation of the result from the exact value, which indicates the precision of the estimation for any function. The error analysis can be accomplished using relative and numerical error analysis methods.^{26,27}

The relative error analysis considers the absolute difference between true investigational (y_{i+1}) and estimated (y_i) values:

$$\epsilon_r = \left(1 - \frac{y_i}{y_{i+1}}\right) \tag{1}$$

The numerical error analysis can be performed using the Euler’s method and the Heun’s 2nd order Runge–Kutta method with step size means given by (x_i, x_{i+1}) and (y_i, y_{i+1}), which are essentially terms from the Taylor series expansion.

The subsequent equations show the derivation of the numerical error using the Euler’s method as follows:

$$y_{i+1} = y_i + f(x_i, y_i)h \tag{2}$$

$$h = y_{i+1} - x_i \tag{3}$$

$$\emptyset = \frac{dy}{dx} = f(x_i, y) = \frac{y_{i+1} - y_i}{x_{i+1} - x_i} \quad (4)$$

$$y_{i+1} = y_i + \emptyset h \quad (5)$$

$$\emptyset h = y_{i+1} - y_i \quad (6)$$

The numerical error is obtained using the Heun's method as follows:

$$y_{i+1} = y_i + \frac{h}{2}(k_1 + k_2) \quad (7)$$

$$k_1 = f(x_i, y_i) \quad (8)$$

$$k_2 = f(x_i + h, y_i + k_1 h) \quad (9)$$

2.3 Simulation of XRD pattern

XRD analysis is a method useful for observing and comparing the structural changes of reduced pyrite ash minerals. Powder diffraction line profiles of XRD patterns can be estimated using Gaussian and Lorentzian shape functions.^{28,29} The width of a line profile is described by the full width at half maximum (FWHM) parameter in simulation modelling. The Gaussian equation comprises the exponential form of the intensity and the theta angle; thus, this model is a fine-estimating function of investigational data.

The Gaussian function is modified to represent XRD profiles as follows:

$$G(x, y) = \frac{1}{2\pi} e^{-\left(\frac{x^2 - y^2}{2}\right)} \quad (10)$$

The Lorentzian function is pertinent profile shape equation, which can also describe tested diffraction line data.

The revised Lorentz function is improved to characterise XRD profiles as follows:

$$L(x, y) = \frac{1}{\sqrt{2\pi}} \left(\frac{1}{x^2} - \frac{1}{y^2} \right) \quad (11)$$

3 Results

The strains of *S. cerevisiae* were well grown in 3 % pulp solutions of calcinated pyrite ash media with constant air temperature and constant feeding. The temperature of the media was kept around 37 °C, and the lowest pH was recorded as 4.5.

The initial, evolving, maximum, and declining counts of *S. cerevisiae* were recorded during the preliminary growth periods in the designed bioprocess; these values were used to generate predicted graph curves. The counts of *S. cerevisiae* indicated a slow growth during the preliminary peri-

od, and the growth declined when the count reached the highest amount (N_m).

3.1 Modelling and error results

All common growth models were surveyed to determine the best assumed fit for the sigmoidal curves in order to describe the investigations of the *S. cerevisiae* counts. For this, the specific growth rate kinetic constants (r) were obtained using the analytical solutions of each modelling equation from the line slope in the population versus time graph. The approximated data were then recalculated using the estimated rate constants. The computed respective rate constants of the models, and the regenerated initial, maximum, and final counts of *S. cerevisiae* are given in Tables 2 and 3, respectively.

Table 2 – Computed values of the growth rate kinetics constants, r

Growth model	r
Exponential	0.0026
Logistic	0.0027
Gompertz	0.0058
Richards	0.0270
von Bertalanffy	0.0008

Table 3 – Computed initial, maximum, and last counts of *S. cerevisiae*

		Counts (10^5 CFU ml ⁻¹)		
		Initial	Maximum	Last
Predicted	Experimental	1.1	5.4	4.6
	Exponential	1.1	3.9	3.4
	Logistic	1.1	4.8	4.3
	Gompertz	7.4	26.5	26.5
	Richards	17.2	22.2	22.2
	von Bertalanffy	1.1	5.3	4.8

Different modelling approaches were examined in this study to extend the investigations and retrieve appropriate displays for each model. Smooth 3D graphs were generated using the number of counts recorded from the experiments, and the predictions were modelled with respect to culture time parameter.

The analytical solution of the exponential function was used to determine the rate constant of the exponential model, which was obtained as 0.0026 from the slope. The approximated initial, maximum, and final counts of *S. cerevisiae* using the exponential rate constant were calculated as $1.1 \cdot 10^5$, $5.4 \cdot 10^5$, $4.7 \cdot 10^5$ CFU ml⁻¹, respectively. The

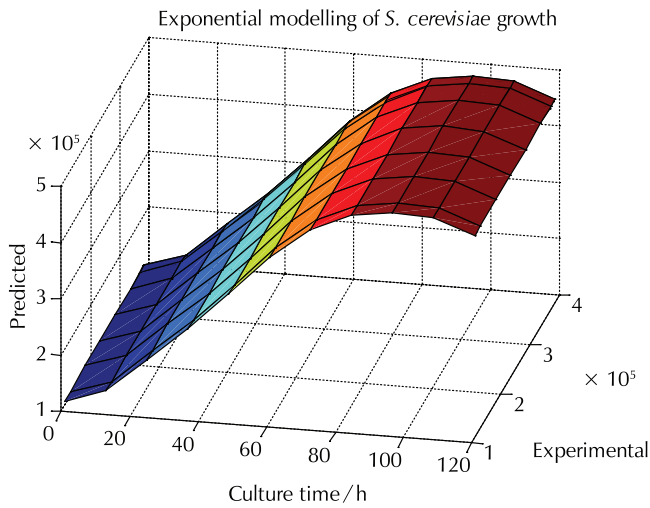


Fig. 1 – Exponential model prediction

exponential modelling results were found comparable to the real value shown in Table 3. Fig. 1 shows the graph of the number of counts obtained from investigations and exponential prediction vs culture time. As the exponential model includes only the initial count (N_0) that does not comprise the growth capacity parameter, it covers only a simplistic expression of the tested data. A sigmoidal fit with errors was obtained with the exponential model. The error analysis for the exponential solution is shown in Fig. 2, which indicates maximum relative error deviation between the real and estimated data of 26.8 %. The analysis of the maximum numerical error using the Euler’s and Heun’s methods yielded errors of 4.8 % and 5.4 %, respectively, which yielded the lowest errors computed.

The maximum number (N_m) of *S. cerevisiae* expresses the carrying capacity, which is considered as the main parameter in the logistic, Gompertz, Richards, and von Bertalanffy modelling functions. The carrying capacity relates viability

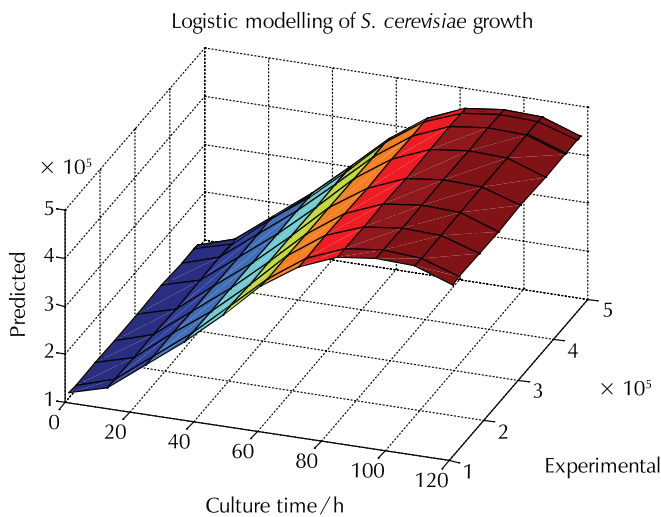


Fig. 3 – Logistic model prediction

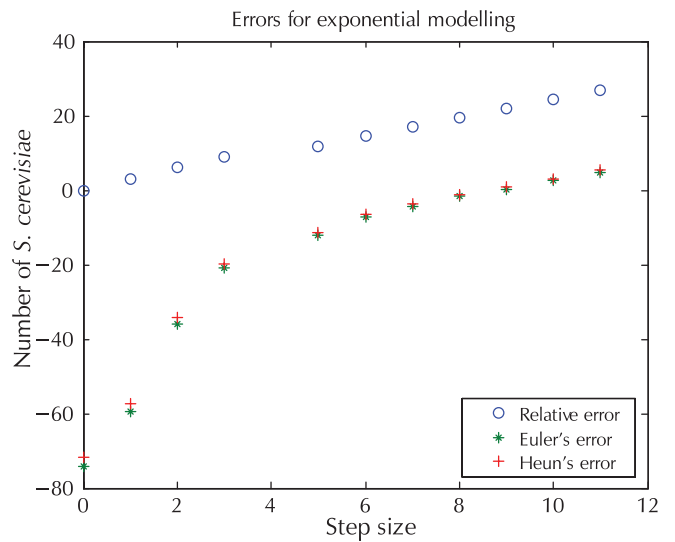


Fig. 2 – Error analysis for the exponential solution

regulation with N_m , which was experimentally detected to be $5.4 \cdot 10^5$ CFU ml⁻¹. The carrying capacity was assessed to sketch a graph to calculate the logistic rate constant, as well as the initial and final counts. The rate constant of the logistic model was determined to be 0.0027 from the slope, and was used to regenerate the logistic investigation data. The initial, maximum, and final counts were determined as $1.1 \cdot 10^5$, $4.8 \cdot 10^5$, and $4.4 \cdot 10^5$ CFU ml⁻¹, respectively, using the logistic rate constant as presented in Table 3. The counts acquired from the observations and the logistic function evaluation with respect to culture time interval are presented in Fig. 3, which shows an S-shaped curve with a maximum relative error of 14.7 %. The maximum numerical errors in the case of the logistic model were estimated as 17.3 % for the Euler’s method, and 64.6 % for the Heun’s method, as seen in Fig. 4.

The Gompertz equation, one of the extended logistic modelling equations, was used to determine the rate con-

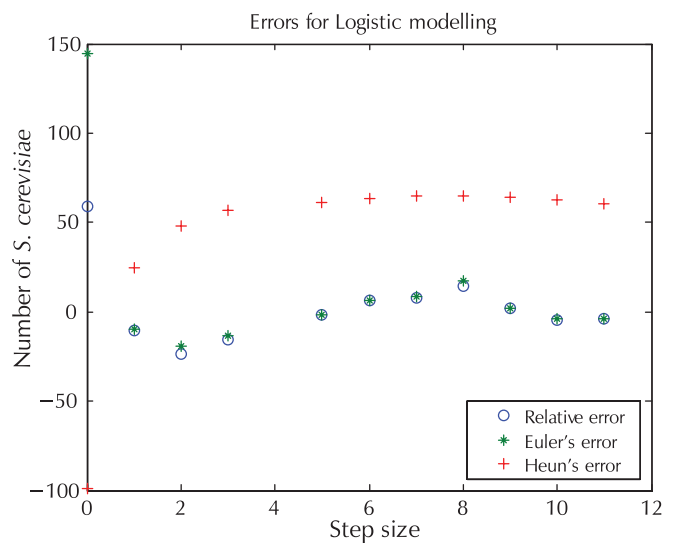


Fig. 4 – Error analysis for logistic model estimation

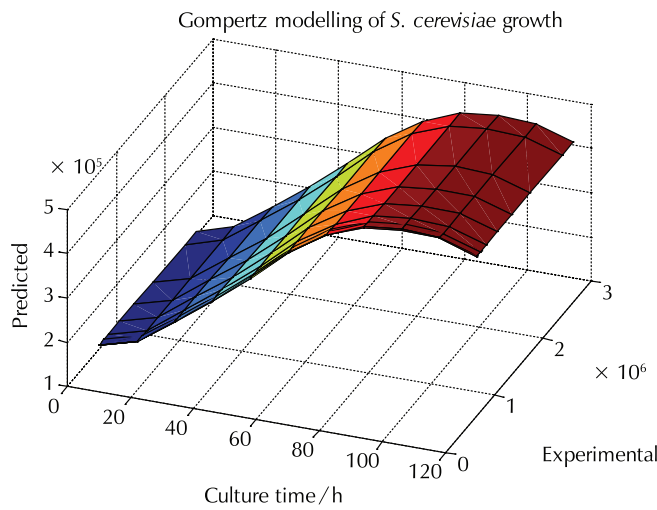


Fig. 5 – Gompertz model prediction

stant, which was determined as 0.0058. This recalculation yielded the predicted initial, maximum, and final counts of $7.4 \cdot 10^5$, $26.5 \cdot 10^5$, and $26.5 \cdot 10^5$ CFU ml⁻¹, respectively, as shown in Table 3. In this table, the initial value of the counts was found to be much higher than the calculated value. The values for the experiments and Gompertz function approximations were recalculated using the Gompertz rate constant, as illustrated in Fig. 5. The maximum relative and numerical error deviations between the observed values and the values estimated using the Gompertz model had a 12.3 % relative error, 14.1 % Euler’s error, and 101.7 % Heun’s error, as shown in Fig. 6.

The Richards and von Bertalanffy restricted modelling equations, after modifications in β , yielded the maximum counts of *S. cerevisiae*. The Richards rate constant was estimated as 0.027, and the initial, maximum, and final counts were determined as $17.2 \cdot 10^5$, $22.2 \cdot 10^5$, and $22.2 \cdot 10^5$ CFU ml⁻¹, respectively, when $\beta = -0.9$ exponential adjust-

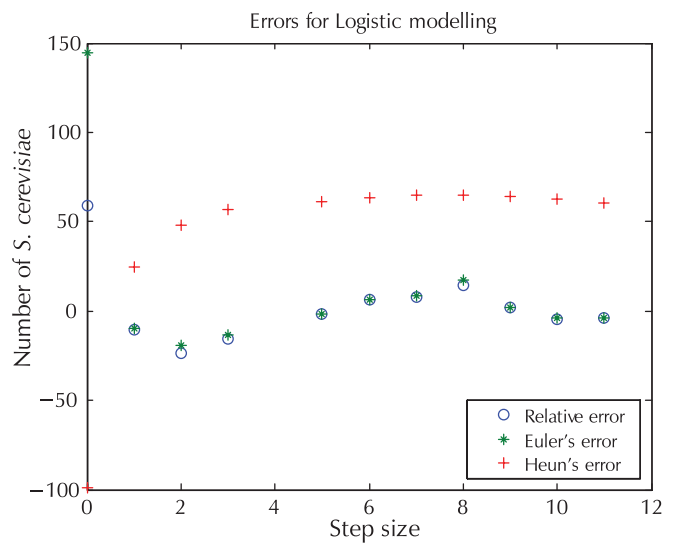


Fig. 6 – Error analysis for the Gompertz model estimation

ment, which was acknowledged as unusual. These results were plotted to obtain a sigmoidal curve as demonstrated in Fig. 7. The maximum errors for the Richards estimations yielded a -2.8 % relative error, -2.7 % Euler’s error, and 105.7 % Heun’s error, as visualised in Fig. 8.

The von Bertalanffy function incorporated with power $\beta = 3$ calculation yielded a rate constant of 0.00084, and the initial, maximum, and final counts were $1.1 \cdot 10^5$, $5.3 \cdot 10^5$, and $4.8 \cdot 10^5$ CFU ml⁻¹, respectively. These counts were found to be comparable values to the observed counts as well as the exponential and logistic estimation data. The sigmoidal curve obtained from the von Bertalanffy function evaluation is illustrated in Fig. 9, which is considered as an identical fit to the real experimental data. The maximum relative error deviation was estimated to be 11.6 %. Furthermore, the Euler’s and Heun’s methods yielded errors of 13.1 % and 101.1 %, respectively, as demonstrated in Fig. 10.

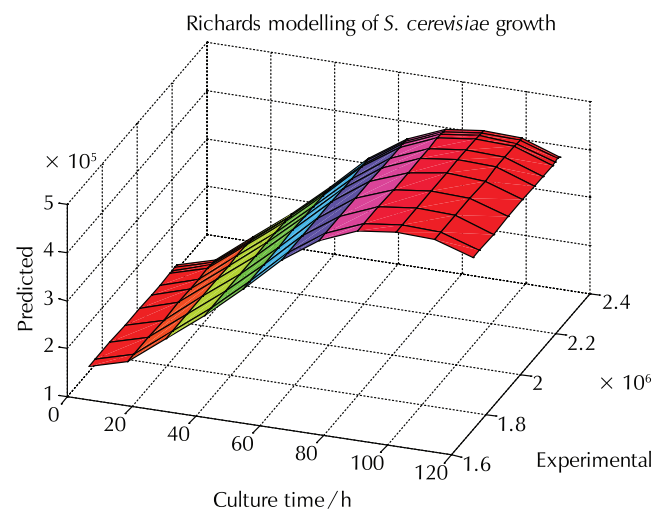


Fig. 7 – Richards model prediction

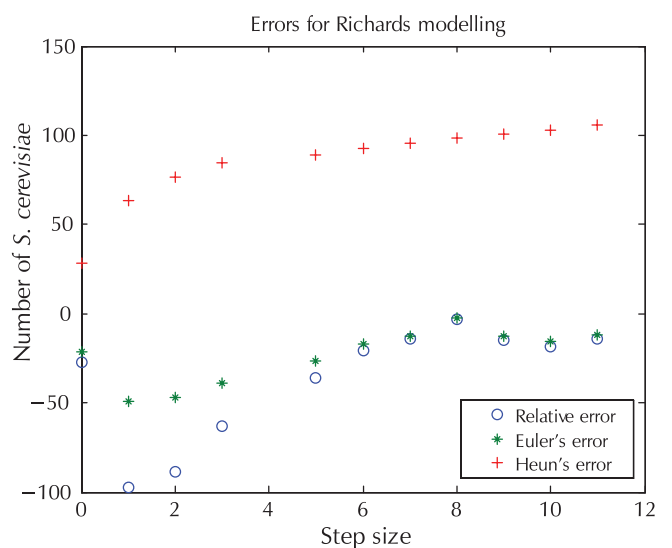


Fig. 8 – Error analysis for the Richards model estimation

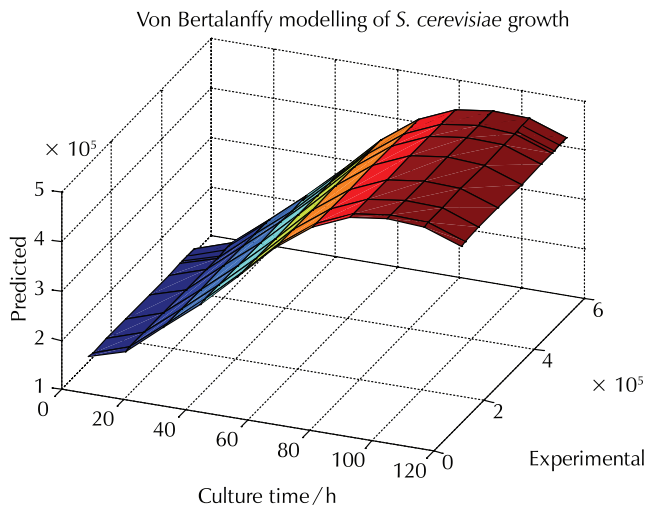


Fig. 9 – Richards model prediction

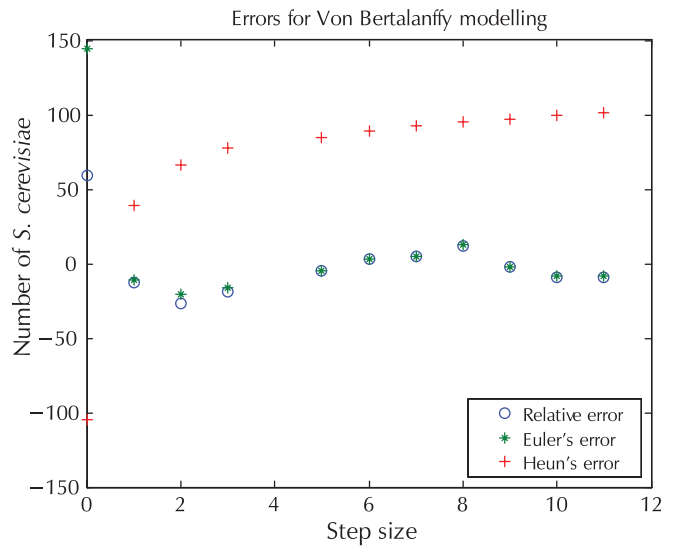


Fig. 10 – Error analysis for the Richards model estimation

The maximum relative error deviation between the real and evaluated data in the exponential model was determined to be 26.8 %. The deviation calculated with the Richards model was estimated as -2.8% , which was considered as unrealistic. The maximum numerical errors calculated using Euler's method Euler's method were 17.3 % for the logistic model, and 105.65 % for the Richards model. The error deviation of the von Bertalanffy method with an approximation of $\beta = 0.1-1.1$ and 0.1 increment, was found to be higher than that of the other modelling equations.

The lowest relative error deviation between the experimental and estimated data was obtained using the von Bertalanffy model solution, yielding a value of 11.6 %. Heun's method yielded the minimum numerical errors of 4.8 % and 5.4 %, respectively, as shown in Table 4.

Table 4 – Maximum error values for the applied models

	Relative error / %	Euler's error / %	Heun's error / %
Exponential solution	26.8	4.8	5.36
Logistic solution	14.73	17.28	64.59
Gompertz solution	12.33	14.06	101.73
Richards solution	-2.80	-2.73	105.65
von Bertalanffy solution	11.56	13.07	101.10

3.2 XRD pattern simulations

The pyrite ash samples were quantitatively studied using XRD analysis, and a slight decomposition was detected in the sulphur-associated minerals, as reported in previous studies.^{2,3}

The initial diffraction profile of the pyrite ash sample was accurately obtained using the actual intensity data as illus-

trated in Fig. 11, in which diffraction line number 5 was attributed to sulphur mineral compounds, such as FeS, PbS, CuS, and PbSO₄. Therefore, the initial and final profiles of line 5 were evaluated as shown in Fig. 12. The areas under the curves in these profiles corresponded to the total intensity of the related molecules, and the difference between the areas under the two curves was attributed to a slight variance in the decompositions. The mineral composition of pyrite ash, as determined through XRD analysis on the first day, is specified in Table 5.

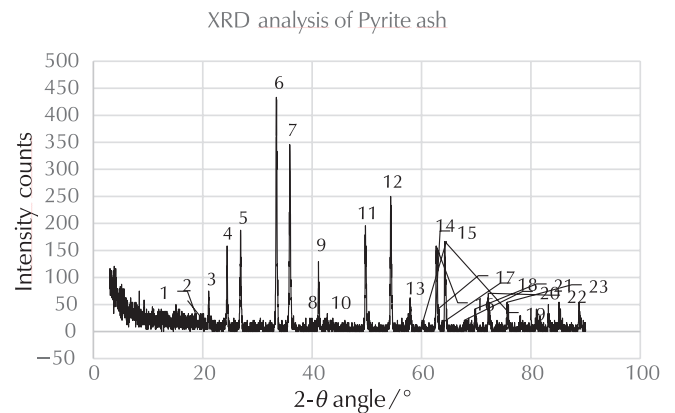


Fig. 11 – Initial day XRD analysis of pyrite ash

As presented in Fig. 12, the initial and final profile data represent the pyrite ash mineral components, and the test results indicated slight decreases in the amounts of sulphur and non-sulphur minerals due to the microbial process, as reflected in the plots of intensity rate against theta. The differences between the two lines are presented in Fig. 13, which shows a trivial difference in the intensity between the initial and final diffraction profile data of line 5. Slight differences between the profiles of line 5 on the initial and final days were also observed, as shown in Fig. 13. The

Table 5 – Mineral molecules of initial day XRD analysis of pyrite ash

Line No.	Mineral Molecules	Line No.	Mineral Molecules
1	FeS	13	ZnO, FeO, Fe ₂ O ₃
2	CuO	14	ZnO
3	CuSO ₄	15	FeO
4	PbSO ₄	16	CuS
5	Fe ₂ O ₃ , FeS, PbS, CuS, PbSO ₄	17	FeO, Fe ₂ O ₃
6	Fe ₂ O ₃ , ZnO	18	ZnO
7	CuO	19	FeS
8	FeS, CuO	20	FeO
9	FeO	21	FeO
10	PbS	22	FeS
11	ZnO, PbO, FeS	23	FeO
12	ZnO, FeO	24	FeO

intensity of the diffraction lines of the constituents of the sample changed after the experiments. The maximum intensities of line 5 on the initial and final days were recorded as 220 and 185, respectively.

Line 5 on the final days was simulated by the Gaussian and Lorentzian functions as 3D simulation graphs presented in Figs. 14 and 15, respectively. As seen in Fig. 14, the diffraction line data were well-fitted roundly using Gaussian function completing the half value of the maximum intensities and yielding the maximum intensity around 220. An incomplete fit was acquired using Lorentzian function resulting in the maximum intensity around 150, as seen in Fig. 15.

4 Discussion

Growth behaviour of *S. cerevisiae* and molecular structure of pyrite ash samples were studied using the growth modelling and XRD pattern simulations.

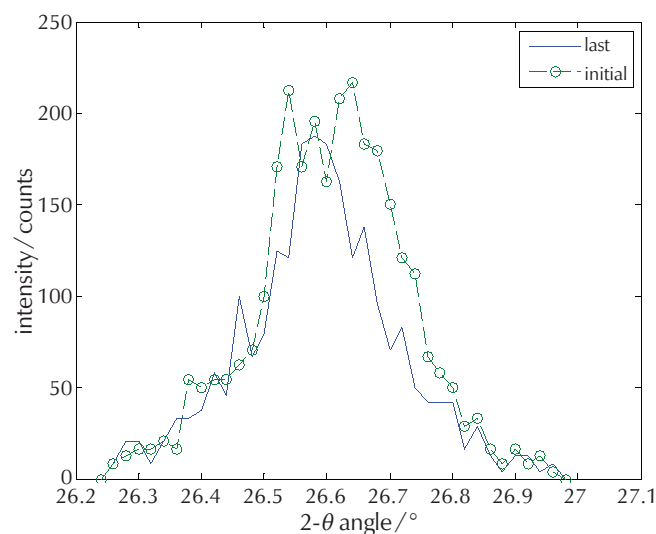


Fig. 12 – Initial and last days of the XRD analysis of the line 5

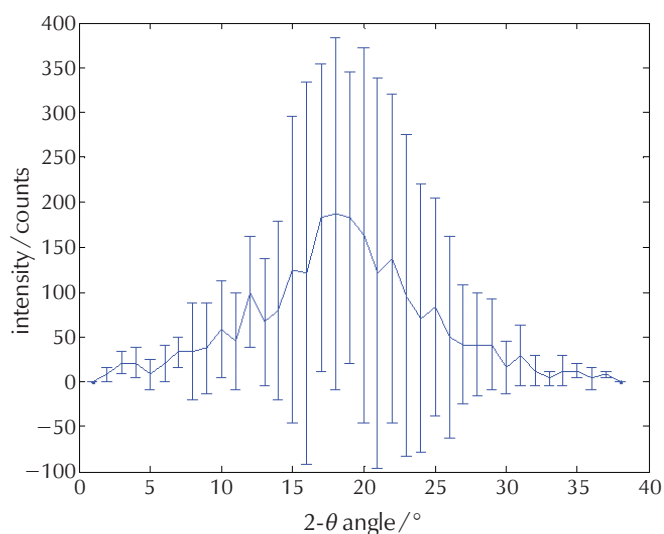


Fig. 13 – Graph of differences between the two lines of the XRD analysis of the line 5

The Gaussian approximation of XRD diffractions

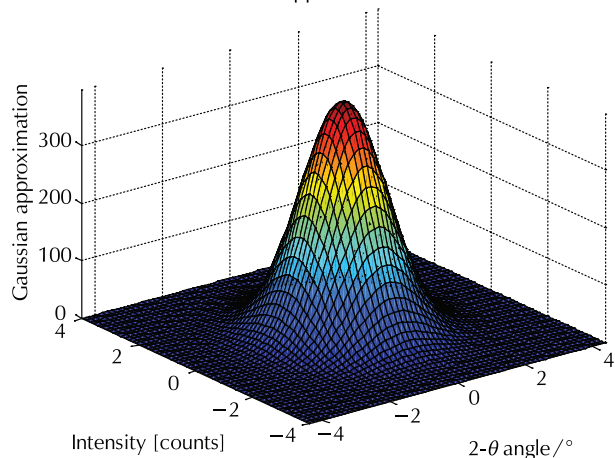


Fig. 14 – Gaussian approximation of XRD analysis of the line number 5

The Lorentz convolution of XRD diffractions

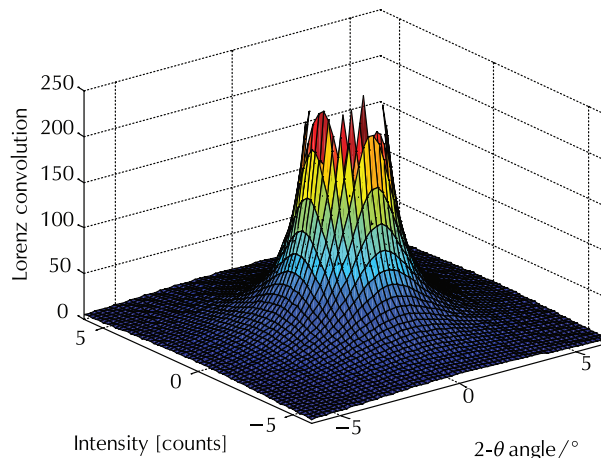


Fig. 15 – Lorentzian approximation of XRD analysis of the line number 5

The observations in this study revealed productive growth and no detectable toxic effect on *S. cerevisiae*; thus, it was deduced that there was no significant heavy metal toxicity during the initial incubation period and a prolonged period for a couple of weeks thereafter. Extended incubation period also led to biofilm layer formation, immobilisation of the microorganisms at the surface of the mineral particles, and biosorption of the smaller particles to the surface of the microorganisms, all of which were detected under microscopic investigations. Habitation of *S. cerevisiae* inside the biofilm layers was observed.

The counts of *S. cerevisiae* as observed through the primary incubation period were substituted in the mathematical expressions of well-known growth models, and the specific growth rate kinetic constants were approximated, as listed in Table 2. Consequently, sigmoidal curves (Figs. 1, 3, 5, 7, and 10) with some errors (Figs. 2, 4, 6, 8, and 10) were obtained, consistent with the results of previous studies.

The rate constants obtained by the exponential and logistic, Gompertz and von Bertalanffy models were used to estimate the initial, maximum, and final counts of *S. cerevisiae*. The counts estimated through these models were the most relevant to the actual counts, whereas the Richards function attained the most irrelevant estimated value, as shown in Table 3. The estimated rate constants, projected figures, and calculated errors specified that all models, except the Richards model, yielded similar results for the initial counts of *S. cerevisiae*.

The graph of the exponential model was drawn using the function and rate constant, yielding the most opposite accuracy compared to the tested data. This accuracy was due to the simplistic N_0 expression of the exponential function. The estimations were repeated using N_m parameter, known as a growth-limiting factor, and the carrying capacity. Moreover, the β power estimations in the other modelling functions yielded lower accuracies than those of the exponential function. Generally, the 3D graphs of the overall models presented S-shaped curves, as shown in Figs. 1, 3, 5, 7, and 9.

The errors between the observed and estimated values of the five models were examined using the relative method and the numerical Euler's and Heun's error methods, as illustrated in Figs. 2, 4, 6, 8, and 10.

The key outcome of this study was that the deviations from the observed values increased depending on N_0 and N_m values, and the β calculations. As seen from the graphs of the surveyed errors, the relative and numerical error analyses for the exponential model approximations yielded in the lowest error percentages, related to the other overall errors. The maximum relative error deviation between the experimental and estimated data for the exponential model was calculated as 26.8 %, whereas the maximum numerical error calculated by the Euler's and Heun's methods were 34.6 % and 61.2 %, respectively. The von Bertalanffy approximation using $\beta = 0.1$ – 1.1 power, yielded the highest error deviation compared to the other modelling estimations.

The lowest relative error deviation between the tested and evaluated data was found to be 11.6 %, which was calculated via the von Bertalanffy model solution. The minimum numerical errors obtained by the Euler's and Heun's methods were 4.8 % and 5.4 %, respectively, as shown in Table 4.

The chemical compositions of pyrite ash have been studied in previous research, and sulphur-containing compounds such as FeS, CuS, CuSO₄, PbS, and PbSO₄ have been detected. The initial and final chemical compositions of the pyrite ash were analysed, and the corresponding XRD analysis results were found to be comparable (Fig. 11). The diffraction line number 5 corresponding to the highest amount of sulphur was selected and investigated specifically through generating graph plots, as well as Gaussian and Lorentzian simulations. The XRD profiles of line 5 on the initial and final days were slightly different (Fig. 12). Fig. 13 demonstrated that the variance between the intensity magnitudes of the two profiles presented the largest discrepancy between the angles of 15°–25°. The diffraction line 5 was described well by the Gaussian function in a 3D simulation, using the tested intensity values, and an analogously fitted shape profile was acquired. Thus, the results revealed a well described relationship between the real and simulated profiles of diffraction intensity and absorption (Fig. 14). However, the Lorentzian function yielded an incomplete fitting result with a sharp edge (Fig. 15).

5 Conclusions

The growth of *S. cerevisiae* was modelled to predict the restrictions and progress of living organisms in the minerals comprising pyrite ash. XRD analysis was performed to examine the mineral decomposition in the incubation bio-process. The *S. cerevisiae* strains could grow well in pyrite mineral ash without heavy metal toxicities. The microorganisms were immobilised on the surface of the mineral ash, and they formed specific types of biofilms. The rate constants were assessed using the analytical solutions of the growth models, and used to regenerate the predicted data for each model equation. The 3D graphs of the five studied models demonstrated S-shaped sigmoidal curves. The lowest relative error was 11.56 %, obtained using the von Bertalanffy model. The models, based on the maximum counts and power estimations yielded weakened model assumptions and increased numerical error deviations. Consequently, the error estimations of Euler's and Heun's methods indicated that the deviation rates increased with model equations that included N_m and β estimations. The numerical methods for exponential model estimation yielded the most appropriate numerical error percentages. Euler's method yielded an error of 4.8 %, whereas Heun's method yielded an error of 5.4 %. The XRD analysis results for the sulphur-containing compounds FeS, CuS, CuSO₄, PbS, and PbSO₄ revealed a slight difference between the initial and final diffraction line profiles. The selected line number 5 was visualised well by the Gaussian function in a 3D simulation, but the Lorentzian function yielded an incomplete fitting result.

References

Literatura

1. N. Tugrul, E. M. Derun, M. B. Pişkin, A. Ekerim, A study on the structural behavior of reduced pyrite ash pellets by XRD and XRF analysis, *Waste Manag. Res.* **27** (2009) 281–287, doi: <https://doi.org/10.1177/0734242X08090404>.
2. H. M. Tsuchiya, A. G. Fredrickson, R. Aris, Dynamics of microbial cell populations. *Adv. Chem. Eng.* **6** (1966) 125–206, doi: [https://doi.org/10.1016/S0065-2377\(08\)60275-6](https://doi.org/10.1016/S0065-2377(08)60275-6).
3. M. L. S. Oliveira, C. R. Ward, M. Izquierdo, C. H. Sampaio, I. A. S. de Brum, R. M. Kautzmann, S. Sabedot, X. Querol, L. F. O. Silva, Chemical composition and minerals in pyrite ash of an abandoned sulphuric acid production plant, *Sci. Total Environ.* **430** (2012) 34–47, doi: <https://doi.org/10.1016/j.scitotenv.2012.04.046>.
4. C. Domènech, À. Canals, A. Soler, A. Sabanès, A. Dumestre, Evolution assessment of soils contaminated by roasted pyrite wastes, *Procedia Environ. Sci.* **17** (2017) 432–435, doi: <http://creativecommons.org/licenses/by-nc-nd/4.0>.
5. M. Gabarrón, O. Babur, J. M. Soriano-Disla, A. Faz, J. A. Acosta, Composition and risk assessment of roasted pyrite ash from fertiliser production, *Chemosphere* **209** (2018) 277–285, doi: <https://doi.org/10.1016/j.chemosphere.2018.06.109>.
6. T. E. Acree, E. P. Sonoff, D. F. Splittstoesser, Effect of yeast strain and type of sulfur compound on hydrogen sulfide production, *Am. J. Enol. Vitic.* **23** (1972) 6–9.
7. R. Stuedel, Mechanism for the formation of elemental sulfur from aqueous sulfide in chemical and microbiological desulfurization processes, *Ind. Eng. Chem. Res.* **35** (1996) 1417–1423, doi: <https://doi.org/10.1021/ie950558t>.
8. H. Sohn, H. Kuriyama, Ultradian metabolic oscillation of *Saccharomyces cerevisiae* during aerobic continuous culture: hydrogen sulphide, a population synchronizer, is produced by sulphite reductase, *Yeast* **18** (2001) 125–135, doi: [https://doi.org/10.1002/1097-0061\(20010130\)18:2<125::AID-YEA655>3.0.CO;2-9](https://doi.org/10.1002/1097-0061(20010130)18:2<125::AID-YEA655>3.0.CO;2-9).
9. A. Mendes-Ferreira, C. Barbosa, V. Falco, C. Leão, A. Mendes-Faia, The production of hydrogen sulphide and other aroma compounds by wine strains of *Saccharomyces cerevisiae* in synthetic media with different nitrogen concentrations, *J. Ind. Microbiol. Biotechnol.* **36** (2009) 571–583, doi: <https://doi.org/10.1007/s10295-009-0527-x>.
10. K. A. Hietala, M. L. Lynch, J. C. Allshouse, C. J. Johns, T. M. Roane, A mathematical model of *Saccharomyces cerevisiae* growth in response to cadmium toxicity, *J. Basic Microbiol.* **46** (2006) 196–202, doi: <https://doi.org/10.1002/jobm.200510061>.
11. D. Brady, J. R. Duncan, Bioaccumulation of metal cations by *Saccharomyces cerevisiae*, *Appl. Microbiol. Biotechnol.* **41** (1994) 149–154, doi: <https://doi.org/10.1007/BF00166098>.
12. J. Wang, C. Chen, Biosorbents for heavy metals removal and their future, *Biotechnol. Adv.* **24** (2006) 427–451, doi: <https://doi.org/10.1016/j.biotechadv.2006.03.001>.
13. F. Di Caprio, P. Altamari, D. Uccelletti, F. Pagnanelli, Mechanistic modelling of copper biosorption by wild type and engineered *Saccharomyces cerevisiae* biomasses, *Chem. Eng. J.* **244** (2014) 561–568, doi: <https://doi.org/10.1016/j.cej.2014.01.098>.
14. J. M. do Nascimento, J. D. de Oliveira, A. C. L. Rizzo, S. G. F. Leite, Biosorption Cu (II) by the yeast *Saccharomyces cerevisiae*, *Biotechnol. Rep.* **21** (2019) e00315, doi: <https://doi.org/10.1016/j.btre.2019.e00315>.
15. D. K. Chaturvedi, Modeling and Simulation of Systems Using MATLAB and Simulink (1st Ed.). CRC Press, Boca Raton, 2010, doi: <https://doi.org/10.1201/9781315218335>.
16. M. Di Serio, R. Tesser, E. Santacesaria, A kinetic and mass transfer model to simulate the growth of baker's yeast in industrial bioreactors, *Chem. Eng. J.* **82** (2001) 347–354, doi: [https://doi.org/10.1016/S1385-8947\(00\)00353-3](https://doi.org/10.1016/S1385-8947(00)00353-3).
17. Y. Ermurat, Modeling the kinetics of pyrite ash biodesulfurization by *Saccharomyces cerevisiae* and *Acetobacter aceti* in liquid state bioreactors, *Electron. J. Biotechnol.* **16** (2013) 1–12, doi: <https://doi.org/10.2225/vol16-issue2-fulltext-1>.
18. A. Laca, C. Quirh, L. A. Garcia, M. Diaz, Modelling and description of internal profiles in immobilized cells systems, *Biochem. Eng. J.* **1** (1998) 225–232, doi: [https://doi.org/10.1016/S1369-703X\(98\)00005-9](https://doi.org/10.1016/S1369-703X(98)00005-9).
19. C. P. Winsor, The Gompertz curve as a growth curve, *P. Natl. A. Sci.* **18** (1932) 1–8, doi: <https://doi.org/10.1073/pnas.18.1.1>.
20. A. H. E. Bijkkerk, R. J. Hall, A mechanistic model of the aerobic growth of *Saccharomyces cerevisiae*, *Biotechnol. Bioeng.* **19** (1977) 267–296, doi: <https://doi.org/10.1002/bit.260190209>.
21. K. W. Szweczyk, A model for baker's yeast growth, *Bioprocess Eng.* **4** (1989) 261–264, doi: <https://doi.org/10.1007/BF00368900>.
22. O. Levenspiel, Modeling in chemical engineering, *Chem. Eng. Sci.* **57** (2002) 22–23, doi: [https://doi.org/10.1016/S0009-2509\(02\)00280-4](https://doi.org/10.1016/S0009-2509(02)00280-4).
23. A. Tsoularis, Analysis of logistic growth models, *Math. Biosci.* **179** (2002) 21–55, doi: [https://doi.org/10.1016/S0025-5564\(02\)00096-2](https://doi.org/10.1016/S0025-5564(02)00096-2).
24. P. R. Koya, A. T. Goshu, Generalized mathematical model for biological growths, *Open J. Math. Model. Simul.* **1** (2013) 42–53, doi: <https://doi.org/10.4236/ojmsi.2013.14008>.
25. N. N. Kulov, L. S. Gordeev, Mathematical modeling in chemical engineering and biotechnology, *Theor. Foun. Chem. Eng.* **48** (2014) 225–229, doi: <https://doi.org/10.1134/S0040579514030099>.
26. Y. Ren, B. Zhang, H. Qiao, A simple Taylor-series expansion method for a class of second kind integral equations, *J. Comput. Appl. Math.* **110** (1999) 15–24, doi: [https://doi.org/10.1016/S0377-0427\(99\)00192-2](https://doi.org/10.1016/S0377-0427(99)00192-2).
27. S. Nakamura, *Applied Numerical Methods*, Prentice Hall, New Jersey, 1993.
28. G. K. Wertheim, M. A. Butler, K. W. West, D. N. E. Buch, Determination of the Gaussian and Lorentzian content of experimental line shapes, *Rev. Sci. Instrum.* **45** (1974) 1369–1371, doi: <https://doi.org/10.1063/1.1686503>.
29. E. J. Mittemeijer, U. Welzel, The “state of the art” of the diffraction analysis of crystallite size and lattice strain, *Z. Kristallogr.* **223** (2008) 552–560, doi: <https://doi.org/10.1524/zkri.2008.1213>.

SAŽETAK

Modeliranje prirasta kulture *Saccharomyces cerevisiae* i simuliranje obrazaca rendgenskog spektra piritnog pepela

Yakup Ermurat

Kvasac *Saccharomyces cerevisiae* inkubiran je u mediju koji je sadržavao piritni pepeo. Uzorci piritnog pepela analizirani su rendgenskom difrakcijskom analizom. Dio rendgenskog spektra koji se odnosio na spojeve koji su u sebi sadržavali atom sumpora simuliran je primjenom Gaussijana i Lorencijana te je uočeno da Gaussijan dobro opisuje eksperimentalne podatke. Za opisivanje prirasta kvasca primijenjeno je više matematičkih modela. Najniža relativna pogreška od 11,56 % dobivena je za von Bertalanffyjev model prirasta. Procjena eksponencijalnim modelom dala je niske vrijednosti postotne pogreške: Eulerova pogreška iznosila je 4,8, a Heunova 5,36 %.

Ključne riječi

Saccharomyces cerevisiae, piritni pepeo, modeliranje prirasta, analiza pogreške, XRD analiza

*Bolu Abant İzzet Baysal University,
Engineering Faculty,
Department of Chemical Engineering,
Bolu, Turska*

Izvorni znanstveni rad
*Prispjelo 12. travnja 2021.
Prihvaćeno 29. kolovoza 2021.*